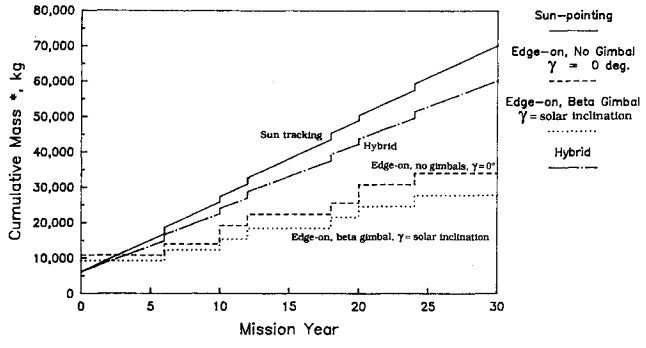

Fig. 2 Mass vs time for various array orientation options for station in 334-km orbit.

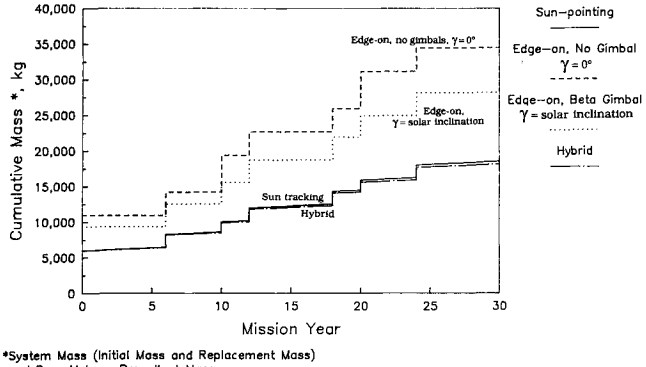

Fig. 3 Mass vs time for various array orientation options for station in 500-km orbit.

Figure 2 shows the cumulative mass to orbit needed for the solar array as a function of years of operation. This accounts for the system mass (including storage and structure) plus the mass of propellant used, assuming $I_{sp} = 445$ s, to cancel the array drag (i.e., not including the portion of the drag which is independent of orientation). The effect of hardware replacement is seen in the abrupt steps at the hardware replacement times. Cumulative mass without the assumption of hardware replacement can be seen by extrapolating the initial portion of the curve. Figure 3 shows the same plot for an assumed 500-km orbit.

Conclusions

The orientation strategy of rotating the array to the edge-on position during the 36-min eclipse period can result in a savings in the required drag makeup propellant of about 18.5% without increasing the array size or changing the configuration.

An array strategy of orienting the array to be always edge on to the flight direction requires the array area to be increased by a factor of two and the storage subsystem to be increased by 50%. This results in higher initial cost and mass but lower 30-year cumulative mass to orbit due to the decreased consumption of propellant. For the 334-km orbit, we calculate that the fully edge-on array orientation reaches a breakeven in mass-to-orbit at about one and a half years against the baseline orientation and at about two years against the edge on during eclipse orientation. For a space station in 500-km orbit, the edge-on configuration has no advantage.

A fully fixed array was examined, but the disadvantages apparently outweigh any advantages.

References

[1]Simon, W. E., and Nored, D. L., "Manned Spacecraft Electrical Power Systems," *Proceedings of the IEEE,* Vol. 75, Institute of Electronics and Electrical Engineers, New York, 1987, pp. 277-307.

[2]Jackson, L. R., Moses, P. L., Scotti, S. J., and Blosser, M. L., "Operational Modules for Space Station Construction," NASA TM 85772, April 1984.

[3]Baraona, C. R., "Space Station Power System," *Space Photovoltaic Research and Technology,* NASA CP 2475, 1986, pp. 321-332.

[4]*Rockwell International, Power System Description Document,* NASA Lewis Research Center, DR:SE-02, Sept. 11, 1987.

[5]Bilardo, V., Jr., and Hudiburg, J., "An Assessment of Nominal and Contingency Altitude Reboost Scenarios During Space Station Assembly," AIAA Paper 88-2638, June 1988.

[6]Lillington, D. R., Kukulka, J. R., Mason, A. V., Sater, B., and Sanchez, J., "Optimization of Silicon 8cm × 8cm Wrapthrough Space Station Solar Cells for On Orbit Operation," *20th IEEE Photovoltaic Specialists Conference,* Institute of Electrical and Electronics Engineers, New York, Sept. 1988, pp. 934-939.

[7]Hough, W. W., and Elrod, B. D., "Solar Array Performance as a Function of Orbital Parameters and Spacecraft Attitude," *Transactions of the ASME, Journal of Engineering for Industry,* Vol. 91, Feb. 1969, pp. 13-20.

[8]Jacchia, L. G., "New Static Models of the Thermosphere and Exosphere with Empirical Temperature Profiles," *Smithsonian Astrophysical Observatory Special Report,* No. 313; also NASA CR-112684, 1970.

Finite Element Analysis of Plasma Flows in Cusped Discharge Chambers

Yoshihiro Arakawa*
University of Tokyo, Tokyo, Japan
and
Paul J. Wilbur†
Colorado State University, Fort Collins, Colorado 80523

Introduction

In a cusped ion thruster, the configuration of the cusped magnetic field applied in the discharge chamber is a design parameter of primary importance because it has a great influence on discharge-chamber performance. A poor field configuration can lead not only to inefficient confinement of primary electrons, but also to a low fraction of the ions produced within the chamber that are extracted into the beam. Some research work to optimize field configurations has been conducted over the last decade, but most of this work has been done experimentally.[1-6] This procedure usually takes a lot of time and is costly because a large number of parameters are involved in chamber designs. Consequently, it is desirable to develop a theoretical model that can be used to suggest the field configuration that will yield optimum discharge-chamber performance.

The objective of this work, as a first step toward developing such a theoretical model, is to apply the finite element method to a simple two-dimensional model describing plasma flows within the discharge chamber for any magnetic field configuration.

Simple Plasma Flow Model

The governing equation for the particle balance within the discharge chamber is

$$-\nabla\cdot([D]\{\nabla n\}) = Q \qquad (1)$$

Presented in part as Paper 88-079 at the DLGR/AIAA/JSASS 20th International Electric Propulsion Conference, Garmisch-Partenkirchen, Germany, Oct. 2-6, 1988; received Jan. 30, 1989; revision received Jan. 17, 1990. Copyright © 1990 by the American Institute of Aeronautics and Astronautics, Inc. All rights reserved.

*Associate Professor, Department of Aeronautics. Member AIAA.
†Professor, Department of Mechanical Engineering. Member AIAA.

where the matrix $[D]$ describes the spatial variation of diffusion coefficients, n is plasma density, and $\{\ \}$ is the vector symbol. When the discharge plasma is assumed to be produced in one-step ionization collisions between primary electrons and neutral atoms, the ion production rate per unit volume Q is given by

$$Q = n_p n_n < \sigma v > \tag{2}$$

Here, n_p and n_n are the densities of primary electrons and neutrals, respectively, and $< \sigma v >$ is the ionization rate coefficient. Because a primary electron has a mean free path that is much longer than the discharge-chamber length, one can treat a primary electron as a collision-free particle in the electrostatic and electromagnetic fields that exist in the chamber. With a collision-free particle orbit theory, n_p can be expressed in terms of the magnetic field vector potential, as described in Ref. 7.

The atom density in the chamber n_n is determined by a neutral atom flow balance on the discharge chamber and is given by

$$n_n = \frac{4\dot{m}\,(1-\eta_u)}{e v_n A_g \phi_n} \tag{3}$$

where $\dot{m}$ is the propellant flow rate expressed in equivalent amperes, η_u the propellant utilization, e the electron charge, v_n the thermal velocity of neutrals, A_g the grid surface area, and ϕ_n the effective transparency of the grids to neutrals.

The migrations of both ions and Maxwellian electrons across and along magnetic field lines are assumed to be described by Bohm diffusion and ambipolar diffusion, respectively. In a coordinate system oriented so that the z' axis is coincident with the tangent to the magnetic field at a point P, the diffusion matrix $[D']$ at P can be written as

$$[D'] = \begin{bmatrix} D_A & 0 \\ 0 & D_B \end{bmatrix} \tag{4}$$

where components D_A and D_B are the ambipolar and Bohm diffusion coefficients, respectively. If we assume that the electron temperature T_e is constant and is much higher than ion temperature, the ambipolar diffusion coefficient can be approximated by

$$D_A = \frac{kT_e}{e} \cdot \mu_i \tag{5}$$

where μ_i, the ion mobility, is inversely proportional to the neutral atom density. The Bohm diffusion coefficient D_B is given by[8]

$$D_B = \frac{kT_e}{16eB} \tag{6}$$

where the magnetic flux density B is a function of position within the discharge chamber and is calculated prior to the plasma flow analysis as a solution to the magnetostatic equations and boundary conditions describing the discharge-chamber magnetic field configuration.

In the r'-z' coordinate system, the plasma diffusion flux vector $\{\Gamma'\}$ is given by

$$\{\Gamma'\} = -[D']\ \{\nabla' n\} \tag{7}$$

When the r'-z' coordinate system is rotated through an angle θ relative to the fixed r-z coordinate system (located with its axes tangent to the discharge-chamber axes) at a position P, one obtains the following relations:

$$\{\Gamma'\} = [R]\ \{\Gamma\} \tag{8}$$

and

$$\{\nabla' n\} = [R]\ \{\nabla n\} \tag{9}$$

where $[R]$ is a rotation matrix at P and is written

$$[R] = \begin{bmatrix} \cos\theta & \sin\theta \\ -\sin\theta & \cos\theta \end{bmatrix} \tag{10}$$

By using the foregoing relations, the diffusion flux vector defined with respect to the r-z coordinates becomes

$$\{\Gamma\} = -[D]\ \{\nabla n\} \tag{11}$$

where

$$[D] = [R]^{-1}[D']\ [R] = \begin{bmatrix} D_{11} & D_{12} \\ D_{21} & D_{22} \end{bmatrix} = \begin{bmatrix} D_A \cos^2\theta + D_B \sin^2\theta & (D_A - D_B)\sin\theta\cos\theta \\ (D_A - D_B)\sin\theta\cos\theta & D_A \sin^2\theta + D_B \cos^2\theta \end{bmatrix} \tag{12}$$

Substituting Eq. (12) into Eq. (1), we obtain the following governing differential equation:

$$\frac{1}{r}\frac{\partial}{\partial r}\left(D_{22} r \frac{\partial n}{\partial r} + D_{21} r \frac{\partial n}{\partial z}\right) + \frac{\partial}{\partial z}\left(D_{12}\frac{\partial n}{\partial r} + D_{11}\frac{\partial n}{\partial z}\right) + Q = 0 \tag{13}$$

Under most operating conditions, the potential of a typical discharge plasma will be higher than that of a chamber wall surface even when the chamber wall serves as an anode. In this case, a sheath will exist not only upstream of the grids but also at the wall surfaces. The ions arriving at the sheath edge should be accelerated to the Bohm velocity v_B (Ref. 9) in order to assure that this sheath will be stable. Consequently, the boundary condition at the chamber and grid surfaces becomes

$$(\{\Gamma\})_n = n_s v_B \tag{14}$$

where $(\{\Gamma\})_n$ represents the vector component of the flux normal to the surface, and n_s is a plasma density at the sheath edge. Because axisymmetric plasmas are being considered in this analysis, the boundary condition on the discharge-chamber axis becomes

$$(\{\Gamma\})_n = 0 \tag{15}$$

In order to solve the aforementioned differential equation [Eq. (13)], the entire domain in the discharge chamber is subdivided into a large number of triangular elements. For each of these elements, the equation is transformed into an algebraic equation using the usual finite element analysis technique.[10]

Numerical Examples

Example 1

Consider the discharge plasma produced in a 20-cm-diam cylindrical discharge chamber having six magnet rings arranged to produce the computed magnetic field configuration shown in Fig. 1. When samarium-cobalt magnets with magnetization $M = 0.83$ T are used, the magnetic circuit analysis yields flux densities that range from 0.23 to 0.28 T at the magnet surfaces and from 20 to 200 mT at the grid surface. Figure 2 shows a plasma density distribution calculated for the case in which the xenon propellant flow rate $\dot{m} = 1$ A-eq, the propellant utilization $\eta_u = 0.8$, the discharge voltage $V_d = 30$ V (correspondingly, the primary electron energy $E_p = 30$ eV), the electron temperature $T_e = 2$ eV, the neutral atom temperature $T_n = 0.05$ eV, and the grid system transparency to neutral atoms $\phi_n = 0.3$. Although a relatively uniform plasma is ob-

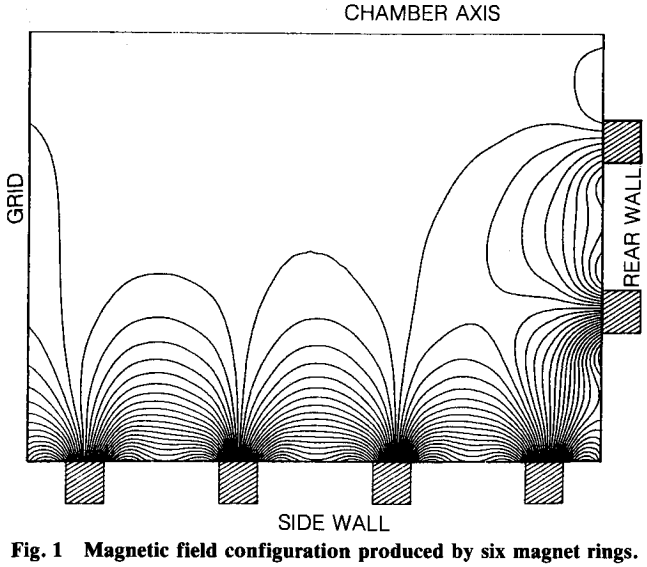

Fig. 1 Magnetic field configuration produced by six magnet rings.

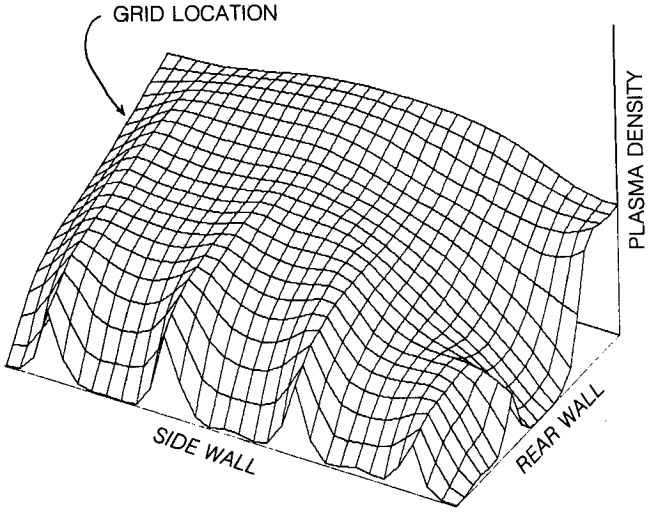

Fig. 2 Plasma density distribution for the magnetic field configuration produced by six magnet rings.

tained in the region near the chamber axis, large density variations are seen over the region near the chamber walls. The distribution at the wall surface has peaks that appear at positions corresponding to the locations of the magnets. This results because, at the center of the cusp, the plasma can escape relatively easily to the surface by flowing along the magnetic field lines of force. In the region between the cusps, Fig. 2 shows that the plasma density at the walls remains low. This result seems reasonable because the strong magnetic fields in these regions inhibit plasma diffusion to the walls. As the ion loss flux density is assumed to be proportional to the plasma density at the wall surface [see Eq. (14)], one can calculate the fractions of ions produced that flow to each surface. In this case, the fractions to the grids f_G, to the side wall f_S, and to the rear wall f_R are 54, 36, and 10%, respectively.

Example 2

This example demonstrates that the present method can be used to investigate the effect of not only field configuration, but also cathode position. In the former example, it was assumed that primary electrons were being emitted from the position where the magnetic vector potential was zero (i.e., all along the chamber axis). When primary electrons are emitted from positions of nonzero potential, the regions of the chamber to which they have access, and where ionization will therefore occur, will also change. Figure 3 shows the effect of changing the radius and axial location of an annular primary electron source (a cathode) on the extracted ion fraction ($f_B = \phi_i \cdot f_G$) for a 9-cm-diam discharge chamber. A grid system transparency to ions (ϕ_i) of 0.75 was used to compute these results. The data show that increasing the cathode radius, so that the electrons are emitted closer to the side wall surface, causes the extracted ion fraction to decrease considerably. When the cathode is located upstream of the axial location of the cusp, the data suggest that primary electrons tend to be trapped by the cusped field and to produce ions locally in the cusp region. In this case, most of the ions produced are lost to the wall surface near the cusp and this results in a very low extracted ion fraction. In Fig. 3, experimental data (obtained from Ref. 11) are also shown for comparison. The calculated results are in qualitative agreement with the experimental ones.

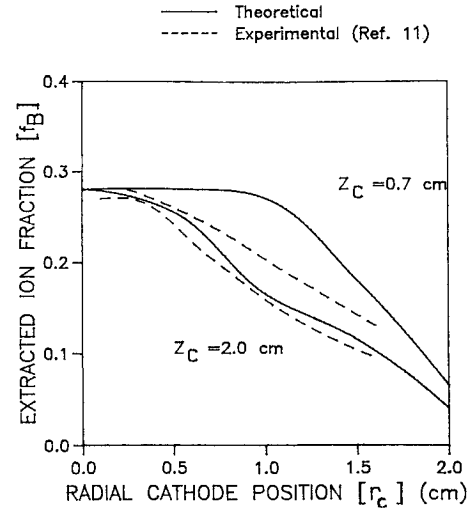

Fig. 3 Effect of cathode position on the extracted ion fraction.

Conclusion

With the finite element method, a simple plasma flow model that can be used to calculate the fractions of ions produced that flow toward the grid and wall surfaces has been developed. Two numerical examples have been employed to demonstrate that this model can be used to obtain plasma density distributions and to calculate the extracted ion fractions for various cusped magnetic field configurations. A logical next step in the development of this model will be to combine the present capability with basic equations describing the conservation of energy, primary and Maxwellian electrons, and ions. A model of this type should facilitate the computation of such discharge-chamber performance parameters as the beam ion energy cost and make it possible to optimize magnetic field geometry and strength for good performance.

References

[1]Ramsey, W. D., "Magnetoelectrostatic Thruster Physical Geometry Tests," *Journal of Spacecraft and Rockets,* Vol. 19, No. 2, 1982, pp. 133–138.

[2]Sovey, J. S., "Performance of a Magnetic Multipole Line-Cusp Argon Ion Thruster," *Journal of Spacecraft and Rockets,* Vol. 19, No. 3, 1982, pp. 257–262.

[3]Brophy, J. R., and Wilbur, P. J., "The Flexible Magnetic Field Thruster," *Journal of Spacecraft and Rockets,* Vol. 20, No. 6, 1983, pp. 611–618.

[4]Brophy, J. R., and Wilbur, P. J., "An Experimental Investigation of Cusped Magnetic Field Discharge Chambers," *AIAA Journal,* Vol. 24, No. 1, 1986, pp. 21–26.

[5]Hiatt, J. M., and Wilbur, P. J., "Ring Cusp Discharge Chamber Performance Optimization," *Journal of Spacecraft and Rockets,* Vol. 2, No. 5, 1986, pp. 390–397.

[6]Vaughn, J. A., and Wilbur, P. J., "Ring Cusp/Hollow Cathode Discharge Chamber Performance Studies," *Proceedings of 20th International Electric Propulsion Conference,* Garmisch-Partenkirchen, Germany, 1988, pp. 364–373.

[7]Arakawa, Y., and Wilbur, P. J., "Dishcharge Plasma Calculations in Cusped Ion Thrusters Using the Finite Element Method," *Proceedings of 20th International Electric Propulsion Conference,* Garmisch-Partenkirchen, Germany, 1988, pp. 460–466.

[8]Chen, F. F., *Introduction to Plasma Physics,* Plenum, New York, 1974, Chap. 5, p. 169.

[9]Bohm, D., *The Characteristics of Electrical Discharges in Magnetic Fields,* edited by A. Guthrie and R. K. Wakerling, McGraw-Hill, New York, 1949, Chap. 3, p. 77.

[10]Burnett, D. S., *Finite Element Analysis,* Addison-Wesley, Reading, MA, 1987.

[11]Wilbur, P. J., "Advanced Electric Propulsion Research," NASA CR-182130, 1988.

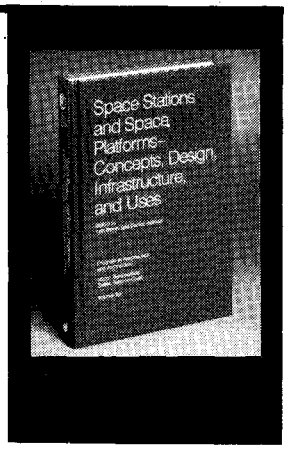

Space Stations and Space Platforms—Concepts, Design, Infrastructure, and Uses

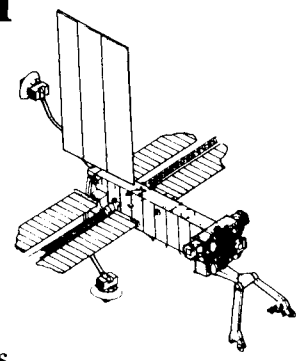

Ivan Bekey and Daniel Herman, editors

This book outlines the history of the quest for a permanent habitat in space; describes present thinking of the relationship between the Space Stations, space platforms, and the overall space program; and treats a number of resultant possibilities about the future of the space program. It covers design concepts as a means of stimulating innovative thinking about space stations and their utilization on the part of scientists, engineers, and students.

To Order, Write, Phone, or FAX:

AIAA

American Institute of Aeronautics and Astronautics
c/o TASCO
9 Jay Gould Ct., P.O. Box 753, Waldorf, MD 20604
Phone (301) 645-5643 Dept. 415 FAX (301) 843-0159

1986 392 pp., illus. Hardback
ISBN 0-930403-01-0 Nonmembers $69.95
Order Number: V-99 AIAA Members $43.95

Postage and handling fee $4.50. Sales tax: CA residents add 7%, DC residents add 6%. Orders under $50 must be prepaid. Foreign orders must be prepaid. Please allow 4-6 weeks for delivery. Prices are subject to change without notice.

945